

---

# Inferring the effect of interventions on COVID-19 transmission networks

Simon Syga<sup>1</sup>, Diana David-Rus<sup>2</sup>, Yannik Schälte<sup>3,4</sup>, Michael Meyer-Hermann<sup>5,6</sup>, Haralampos Hatzikirou<sup>1,7</sup>, Andreas Deutsch<sup>1,\*</sup>

**1 Center for Information Services and High Performance Computing, Technische Universität Dresden, Nöthnitzer Straße 46, 01062 Dresden, Germany**

**2 Bavarian Health and Food Safety State Authority (LGL) – Research division, Veterinärstraße 2, 85764, Oberschleißheim, Germany**

**3 Institute of Computational Biology, Helmholtz Zentrum München – German Research Center for Environmental Health, 85764 Neuherberg, Germany**

**4 Center for Mathematics, Technische Universität München, 85748 Garching, Germany**

**5 Department of Systems Immunology and Braunschweig Integrated Centre of Systems Biology (BRICS), Helmholtz Centre for Infection Research, Braunschweig, Germany**

**6 Institute for Biochemistry, Biotechnology and Bioinformatics, Technische Universität Braunschweig, Braunschweig, Germany**

**7 Mathematics Department, Khalifa University, P.O. Box 127788, Abu Dhabi, UAE**

\*andreas.deutsch@tu-dresden.de

**One sentence summary:** Government interventions should target non-local contacts in order to efficiently prevent disease spread.

## Abstract

Countries around the world implemented non-pharmaceutical interventions (NPIs) to flatten the curve of COVID-19 cases but failed to eradicate the disease. Design of efficient NPIs requires identification of the structure of the underlying transmission network. We combine Bayesian parameter inference with a network-based epidemiological model that allows to interpolate between random and small-world transmission networks. Using epidemiological data from Germany, we show that NPIs reduced non-local contacts in the transmission network, resulting in a change from an exponential to a constant regime. Due to the small-world nature of the inferred network, exponential spread can be efficiently prevented by reducing non-local contacts. Eliminating the disease remains costly as it requires to reduce all contacts. Our code is freely available and can be readily adapted to any country.

## Introduction

The SARS-CoV-2 pandemic has dramatic consequences at a global scale. Since effective treatments and vaccines are still unavailable, many countries have applied

---

non-pharmaceutical interventions (NPIs) of varying severity, like cancelling big events, closing schools, and shutting down businesses to reduce virus transmission by limiting contacts in the population. The prime goal of NPI design is to prevent those contacts in the population which contribute the most to disease spread while allowing less dangerous contacts. Data from several countries indicate that the effect of early, less strict NPIs, like cancellation of large events, had a profound effect on the spread of the disease [1, 2]. Other findings suggest that only a full lockdown reduced the spread noticeably [3], although the implementation of the lockdown varied dramatically between individual countries. For example, Germany did not implement a full lockdown but enacted contact restrictions and closure of non-essential businesses so that people were still allowed to leave their homes and meet in small groups. In several countries, following the implementations of various NPIs, the curves of cumulative infections left the exponential regime and entered a linear one, corresponding to a constant regime of new infections, and an effective reproduction number around 1, see Fig. 1A-C. This is remarkable, because these countries are very heterogeneous regarding their demographics, economic situation and the implemented NPIs. Epidemiological models that assume an underlying random transmission network predict this behavior only for a particularly fine-tuned set of parameters, which contrasts with the robustness of the decline in the reproduction number observed in reality [2, 4–6]. Identification of the underlying transmission network is not only crucial for the design of effective NPIs, but also for assessing other properties of COVID-19 spread, such as the herd immunity threshold [7]. Thurner et al. suggested that the linear regime of cumulative infections is a consequence of a small-world transmission network [8], see Fig. 1D-I. The heterogeneous topology of real social networks is reflected by a small average path length between any two nodes (small world property) and by a power-law distribution (scale-free property) of the node degree [9, 10]. Network-based epidemiological models allow to consider the effects of heterogeneity with respect to the type and frequency of contacts in the population, i. e. how often people meet and whom, by representing all agents as nodes of a network and the contacts in the population by links between these nodes [11–13]. The spread of diseases is strengthened on scale-free networks and the epidemic processes on such networks do not possess epidemic thresholds so that they always produce a major epidemic outbreak [14, 15]. Consequently, on a scale-free network topology the disease is persistent no matter the infection rate [16]. A similar model was able to explain the disease dynamics during the SARS outbreak in Hong Kong in 2003 [17]. Recently, Komarova et. al. discussed the power law behavior of the dynamics of COVID-19 spread in the context of a metapopulation model [18]. We combine Bayesian parameter inference [19] with a network-based epidemiological model that allows to interpolate between random and small-world transmission networks to infer the topology of the transmission network in Germany during three time periods: February 26 until March 15, before serious NPIs were imposed, March 16 until June 6, when strict contact restrictions were in place and non-essential businesses were closed, and June 7 until September 15, when most NPIs were lifted. We show that NPIs reduced non-local contacts in the transmission network, resulting in a change from an exponential to a constant regime of new cases. Non-local contacts often span a large distance in the transmission network and connect different cliques. They include for example contacts during public transport, in bars and restaurants, but also contacts to relatives that live far away. Furthermore, given the nature of non-local contacts, the probability for superspreader events increases when there is a high density of such non-local contacts, as they enable the disease to spread to fully susceptible interconnected cliques. Moreover, reduction of non-local contacts has a strong non-linear effect on the effective reproduction rate and the peak value of infected people, pushing the disease dynamics into a regime of a constant number of new infections.

---

Decreasing the total number of contacts including those within connected cliques, on the other hand, has a strong effect if the epidemic threshold is reached or if the network is almost random, see Fig. 1D,G. Furthermore, we are able to analytically predict disease spread in the absence of non-local contacts by a wave equation where the wave speed (proportional to the growth rate)  $c$  scales as  $c \propto k^2\sqrt{k}$ , where  $k$  is the number of local contacts. This corresponds to the linear spreading regime. In summary, our model suggests that the prime goal of NPIs should be to decrease non-local contacts in the population to prevent an exponential disease spread.

## Results

### Bayesian parameter inference

We aimed to infer the induced changes in the topology of the COVID-19 transmission network by Bayesian parameter inference. We expected that NPIs lead to a change in the behavior of people and therefore in the topology of the corresponding transmission network. We assumed that the transmission network can be described by the Watts-Strogatz network [9] that can interpolate between a random and a small-world network (Supplementary material). Crucially, in this framework, we could distinguish local contacts within cliques, like households, nursing homes, businesses etc. and non-local contacts outside of these clusters, corresponding to encounters in public transport, with business partners, friends and family that live far away and similar. During the construction of the Watts-Strogatz network,  $n$  nodes are placed in a ring topology and connected to their  $k = 2, 4, 6, \dots$  nearest neighbors (local contacts). After that, each link is rewired with a probability  $p$  to another random node (see Fig. S1), and we refer to these links as non-local. We used the SEIR (susceptible-exposed-infectious-removed) epidemiological model for the COVID-19 disease dynamics. Agents in the SEIR model were represented by the network nodes such that infectious agents could spread the disease with probability  $p_I$  to susceptible agents that they are connected to in discrete time steps of single days (Supplementary material, Fig. S2).

We inferred the model parameters  $p, k, p_I$  for the time periods before and after the first NPIs were implemented in Germany, and after most NPIs were lifted again by applying an approximate Bayesian computation with sequential Monte Carlo (ABC-SMC) algorithm (Supplementary material). We did not infer those SEIR model parameters corresponding to the disease progression, which were reported in the literature [21] (Supplementary material) and kept the number of agents fixed at  $n = 3 \times 10^5$ . For the time periods before June 6 when a large number of infections was not reported, we also inferred the initial numbers of exposed and infectious individuals  $n_E(0), n_I(0)$ .

Based on Google mobility reports and previous work on the inference of change points in the spread of COVID-19 [2, 22] we assumed the critical time point for the effect of NPIs in Germany to be March 15, as from March 16, NPIs were synchronized in German states, and schools and non-essential businesses were closed.

We intentionally chose broad, uninformative priors for all parameters, such that we could compare the obtained posterior distributions with other data sources as a sanity-check of our approach. To account for the weekday-dependent reporting delay we used a seven day rolling average of new case reports provided by John Hopkins University [20]. Our parameter inference scheme is based on a minimization of the difference between this average and the number of agents becoming infectious in the model on the corresponding day. We here assumed that all people that were tested positive were also infectious at the time of the test and that the time delay between

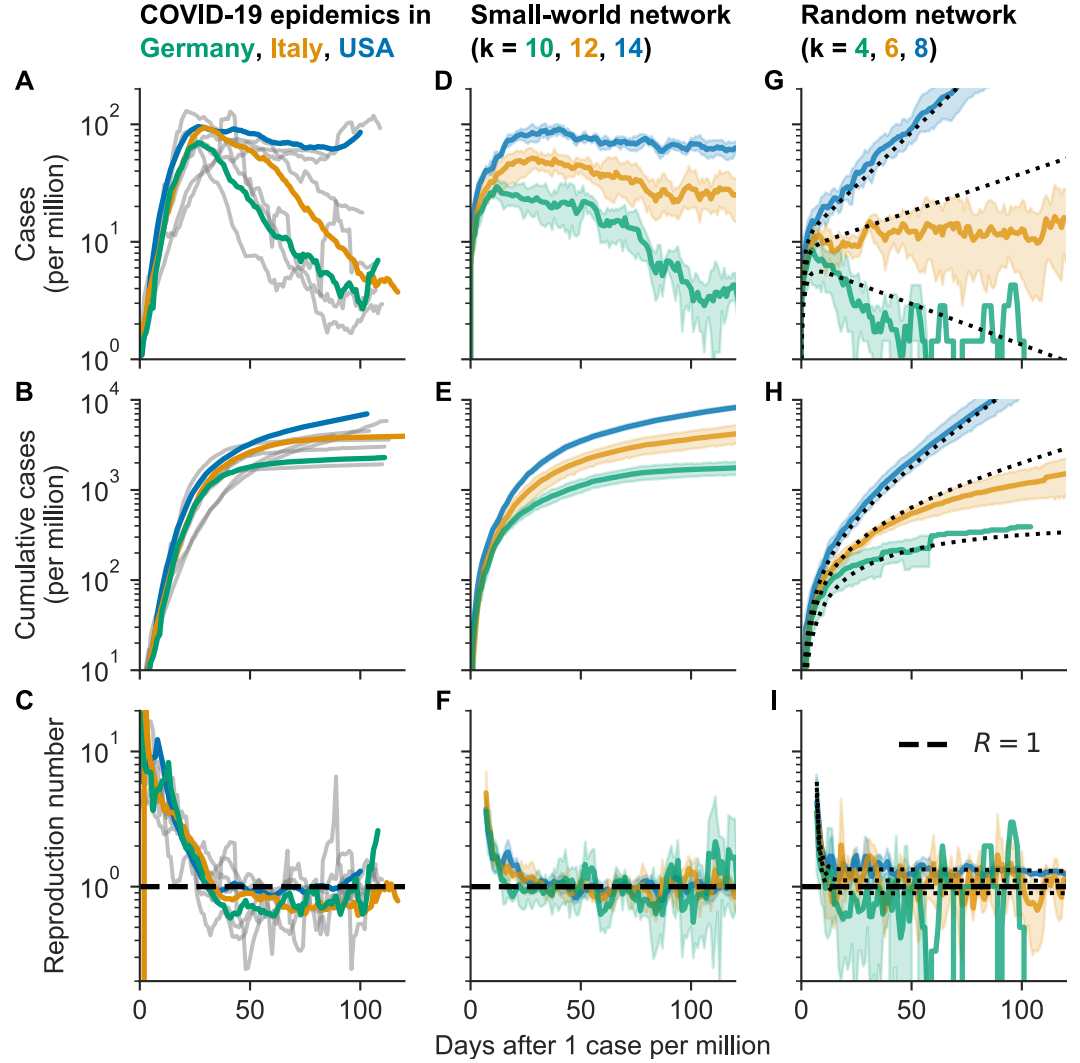


**Figure 1. Dynamics of COVID-19 epidemics could be explained by small-world transmission networks.** (A-C) New cases per million, cumulative cases per million and reproduction number in Germany, Italy and the US. Gray lines are other countries for comparison. After the implementation of NPIs, the case numbers decrease slowly, corresponding to an effective reproduction number of just below 1. Own visualization of data from John Hopkins University [20]. (D-F) Disease dynamics in a clustered small-world network ( $p \approx 0$ ). After an initial exponential increase in cases, new cases are almost constant over time, corresponding to a linear increase in cumulative cases and reproduction numbers around 1. This behavior is robust against changes in the total number of contacts  $k$  and the infection probability  $p_I$ . (G-I) Disease dynamics in a random network. New cases and cumulative cases change exponentially over time, strongly depending on the number of contacts and the infection probability. The reproduction number is equal to one only for a fine-tuned set of parameters. Black dotted lines correspond to predictions of the respective ODE approximation (see Supplementary Material). (D-I) show mean and standard deviation of 5 independent simulations per parameter set on Watts-Strogatz small-world networks with  $n = 10^5$  nodes.

---

people turning infectious and their test is negligible.

First, we inferred the parameters for the time from February 26 to March 15, since daily new cases increased rapidly after February 26, while there were almost no cases in the week before. Our analysis of this time period revealed an almost random transmission network, with a median fraction of non-local contacts of  $p = 0.48$  (with 95 % credibility interval, CI [0.23, 0.94]), a large number of contacts  $k = 26$  (CI [22, 32]) and a high infection probability of  $p_I = 0.035$  (CI [0.025, 0.061]). For the initial condition we estimated that 33 (CI [4, 46]) people were exposed and 81 (CI [32, 118]) people were infectious on February 26.

To assess the changes of the transmission network induced by the NPIs in Germany, we next considered the time period following March 16. During that time frame the NPIs were changed several times, however, the contact restrictions, which we regard as the most crucial intervention, were only lifted on June 6, which is why we chose this date as the endpoint of the time interval. As the total number of cases was computationally intractable, we instead used the relative number of new cases as input for this time period (Supplementary material).

Our Bayesian parameter inference reveals that the NPIs reduced the number of contacts in the transmission network considerably to  $k = 6$  (CI [4, 10]). They also reduced the infection probability of these contacts to  $p_I = 0.02$  (CI [0.010, 0.039]), which matches well with an estimation based on the individual-level secondary attack rate in the household of 17 % [23] (Supplementary material). Crucially, the fraction of non-local contacts decreased to  $p = 7 \times 10^{-5}$  (CI [ $10^{-7}$ , 0.12]), stopping the exponential growth. Additionally, we estimated the number of exposed people on March 16 to be  $n_E(\text{March16}) = 78$  (CI [31, 147]) per million and the number of infectious people to be  $n_I(\text{March16}) = 452$  (CI [301, 656]) per million. The fact that during the week before March 16 there were only 57 infections per million detected in Germany is a hint that a large fraction of infections went unnoticed at the time, which agrees with other reports [24].

We also inferred the model parameters for the time period following June 6 when contact restrictions were lifted. To this end, we used the final time point of simulation instances from the previous time period as initial condition. For the number of contacts we obtained a median  $k = 12$  (CI [6, 20]) that matches well with reports of the average number of daily contacts in Europe of 13.4 [25]. The median fraction of non-local contacts was estimated as  $p = 0.03$  (CI [0.001, 0.6]), which means it was notably smaller than before NPIs had been implemented, but larger than in the time period of strict NPIs. Interestingly, we found that the infection probability was as low in this time period at  $p_I = 0.02$  (CI [0.01, 0.04]) as during the lockdown, which could be the result of a seasonal effect and of people spending more time outside, which hinders the spread of airborne diseases such as COVID-19. We inferred rather broad parameter posterior distributions for this time period, due to the generally low number of infections and large localized outbreaks. Also, for the time periods without strict NPIs (February 26 to March 15 and June 6 to September 15), for which we inferred a large fraction of non-local contacts, the infection probability  $p_I$  and the number of contacts  $k$  were notably correlated, leading to broader posterior distributions. The prior and posterior parameter distributions of the network parameters and the infection probability for the three time periods are shown in Fig. 2.

## Disease dynamics in the small-world network

To determine precisely the transitions between the linear and exponential regimes of the disease dynamics, we performed a parameter scan varying the network parameters  $p$  and  $k$ , while keeping the disease-specific parameters and the system size fixed at  $n = 10^5$ ,  $p_I = 0.02$ . Thereby, reducing  $k$  corresponds to reducing the total number of

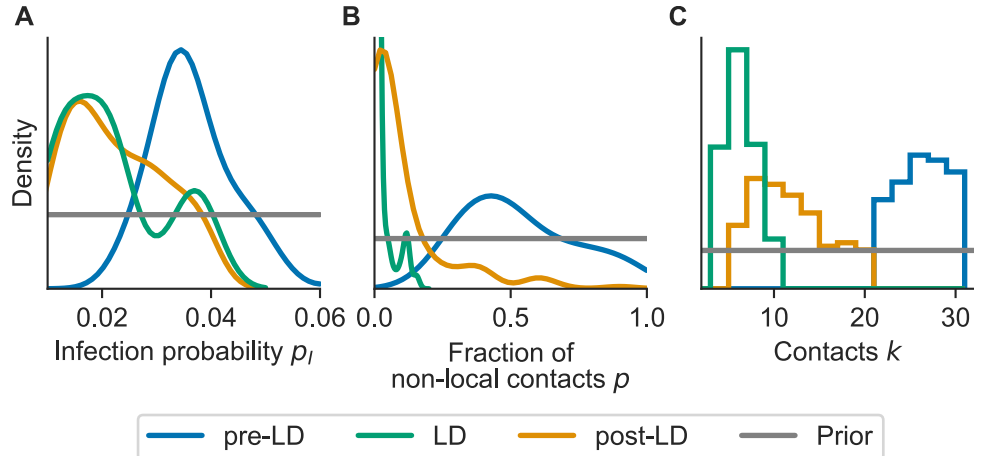


**Figure 2. Inference of central epidemiological parameters before (pre-LD, blue), during (LD, green) and after (post-LD, yellow) the lockdown in Germany.** Shown are kernel density estimates of the posterior parameter distributions of the three time periods and the uniform prior distribution (gray). (A) The infection probability  $p_I$  reduced from  $p_I = 0.035$  (CI [0.025, 0.061]) pre-lockdown to  $p_I = 0.02$  (CI [0.01, 0.04]) during the lockdown. After most restrictions were lifted, the infection probability remained almost unchanged at  $p_I = 0.02$  (CI [0.01, 0.04]). (B) The fraction of non-local contacts in the transmission network  $p$  reduced strongly from  $p = 0.48$  (CI [0.23, 0.94]) to  $p = 8 \times 10^{-5}$  (CI [ $10^{-7}$ , 0.12]) when restrictions were put in place and increased to  $p = 0.03$  (CI [0.001, 0.60]) when they were lifted. (C) The total number of contacts  $k$  decreased strongly from  $k = 26$  (CI [22, 32]) to  $k = 6$  (CI [4, 10]) during lockdown before increasing again to  $k = 12$  (CI [6, 20]) after restrictions were lifted.

contacts (local and non-local), while reducing  $p$  does not change the number of contacts, but restricts them to locally clustered agents (cliques). We recorded the peak number of simultaneously infected people, because a central goal of NPIs is to prevent the overload of the health system, and the total number of infected people after 100 days as a measure for the total damage to public health, see Fig. 3.

Importantly, the number of infections could be reduced massively by only decreasing the fraction of non-local contacts in the population, while keeping the total number of contacts constant. As we have inferred the parameters of the transmission network for different time periods, we could associate them with regions in our parameter space. If no NPIs had been implemented and people would not have changed their behavior, more than 40 % of people could have been infected simultaneously and almost everybody would have been infected after one year (Fig. 3, blue square). The peak was reduced to 0.0002 % by the interventions (Fig. 3A, green point). Lifting the NPIs, moved the system back into the exponential regime, with a projected peak of infections of 1.3 % and almost 10 % of the population to be infected within one year (Fig. 3, yellow diamond). As we have shown, reducing the number of contacts can in principle push the system below the epidemiological threshold leading to extinction of the disease (see Figs. 1, 3), however the effect is weaker in the regime far away from the threshold (see Figs. 1, 3,  $k = 10, 12, 14$ ). On the other hand, in the small world regime  $p \approx 0$ , increasing the fraction of non-local contacts has a dramatic effect: both the peak value of infected agents and the total number of infected agents increase in a non-linear manner. Preventing most non-local contacts in the network ( $p \rightarrow 0$ ) hinders the spread of the disease, so that the effective reproduction number fluctuates around 1, and the cumulative number of infections increases linearly with time as observed in many

countries after the first NPIs were imposed.

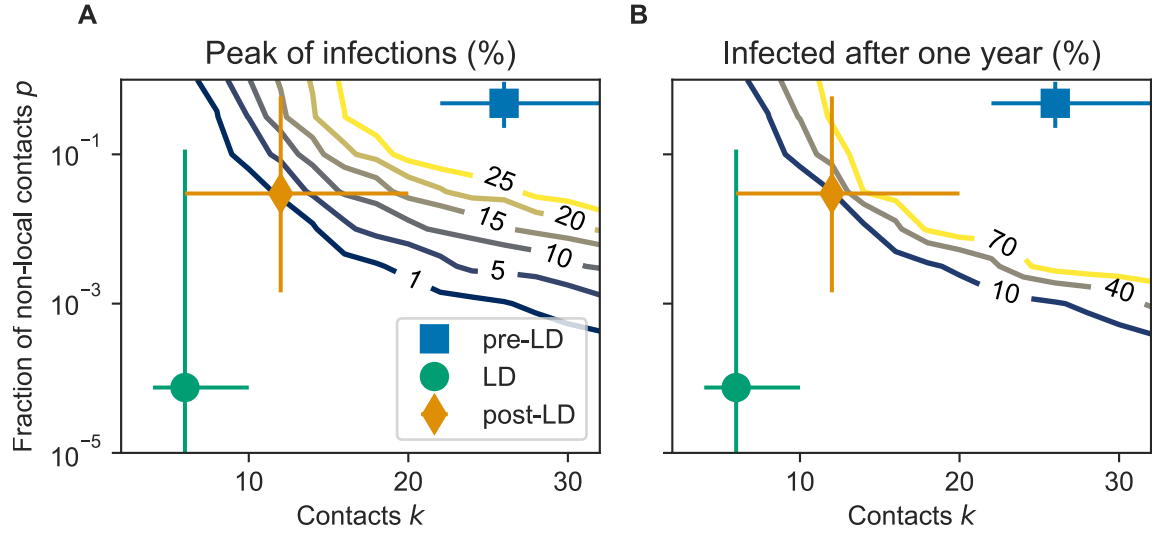


**Figure 3. Preventing non-local contacts can massively mitigate the disease outbreak.** (A) Number of simultaneously infected people (peak of infections) in percent of population. The wave peak can be massively mitigated by decreasing the fraction of non-local contacts, while keeping the total number of contacts constant. (B) Cumulative number of infections after one year in percent of the population. Similar to the peak of infections, the cumulative number of infections can be limited by reducing the fraction of non-local contacts. Blue square (pre-LD), green point (LD) and yellow diamond (post-LD) correspond to the median parameters and 95 % CI obtained from Bayesian parameter inference for the time periods 26/02–15/03, 16/03–05/06 and 06/06–15/09, respectively. The NPIs after March 15 prevented an exponential spread of the disease, but lifting them led to another exponential increase. Shown are contour lines of the mean of 20 independent realizations of each parameter combination  $(p, k)$ , while the other parameters were fixed at  $n = 10^5, p_I = 0.02$ .

### Wave speed of infections in the linear regime

We were especially interested in the disease dynamics in the regime  $p \rightarrow 0$ , as this is where traditional epidemiological models that assume a random transmission network break down. In the case of only local contacts in the network, the disease spreads like a wave originating from the initially infectious agent. This wave-like disease spread was also reported in real networks, such as the air traffic network [26]. In order to calculate the speed of the infection wave, we used a mean-field approximation of an SIR-like agent-based model operating on the Watts-Strogatz small-world network. We scaled the mean-field equations to continuous time  $t$  and space  $x$  (where the distance is measured as the number of links along the ring of nodes), and approximated the dynamics by a set of partial differential equations for the probability densities of susceptible  $\sigma(x, t)$ , infectious  $\iota(x, t)$  and removed  $\rho(x, t)$  agents (see Supplementary material). In particular, we obtained for the probability density of infectious agents

$$\partial_t \iota = \kappa_I \sigma \left[ k(1-p) \left( \iota + \tilde{k} \partial_{xx} \iota \right) + kpI \right] - \kappa_R \iota, \quad \iota + \sigma + \rho = 1, \quad (1)$$

where  $\kappa_I$  is the infection rate,  $\kappa_R$  is the removal rate and  $\tilde{k} := k(k/2 + 1)(k + 1)/12$ . The total number of infectious agents  $I$  is defined as  $I := \int \iota dx$ , where the integral

represents the non-local coupling by non-local contacts. This equation resembles the Fisher-KPP equation [27] but with a non-local coupling and non-linear diffusion term. We recover the classical SIR model for  $p = 1$ , as expected. For the regime  $p = 0$ , we calculated the minimal speed of disease spread through the network as

$$c_{\min} = 2\sqrt{k\kappa_I\tilde{k}(k\kappa_I - \kappa_R)} \propto k^2\sqrt{k}. \quad (2)$$

Notably, the wave speed depends on  $k$  in a highly non-linear way. Comparing our prediction against simulation data of our parameter scan revealed that the wave speed is proportional to the growth rate of the cumulative infections in the linear regime, see Fig. 4.

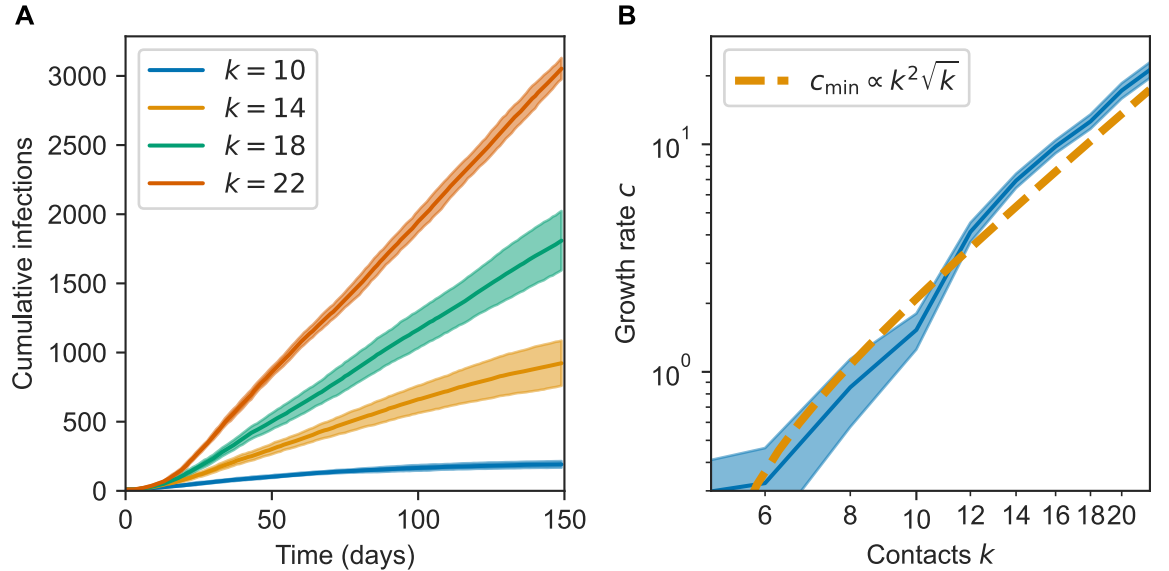


**Figure 4. The growth rate of the cumulative number of infections in the linear regime can be predicted analytically.** (A) Cumulative number of infections in the linear regime ( $p = 0$ ) in the network-based model. (B) Growth rate of cumulative infections in dependence of the number of contacts  $k$ . The growth rate scales as  $c \propto k^2\sqrt{k}$  as predicted by eq. 2. Shown is the mean and standard error of the mean (SEM) of 20 independent simulations for each parameter.

## Discussion

We used Bayesian parameter inference to estimate the effect of government interventions in Germany on the transmission network of COVID-19 assuming it can be approximated by the Watts-Strogatz network. Our analysis revealed that NPIs lead to a reduction in transmission probability, number of contacts, and, crucially, to the removal of almost all contacts outside highly clustered cliques, like households and businesses. In contrast to standard epidemiological models, in this regime the cumulative number of infections does not increase exponentially but linearly, with a massively reduced peak of infections. The dynamics corresponds to a wave-like spread of the disease in the network, whose wave speed  $c$  we predicted by mean-field theory to scale as  $c \propto k^2\sqrt{k}$  in dependence of the number of contacts  $k$ . At the same time, the effective reproduction number fluctuates around 1, irrespective of the wave speed, and is therefore not a useful

---

observable any more. However, as long as the epidemic threshold is not reached by reduction of contacts between cliques and reduction of infection probability, the disease still spreads in the population, which underlines the need for an effective test, trace, and isolate (TTI) system and, ultimately, a vaccine. In our model we assumed a Watts-Strogatz transmission network and therefore assigned non-local links randomly. However, in real social networks, such contacts preferentially link to hubs with a large number of connections potentially connecting several communities, like grocery stores, restaurants, religious establishments etc. This results in a scale-free degree distribution of the network that favors disease spread even more than randomly assigned non-local links and can lead to outbursts of infections (superspreading events) [17]. Our parameter inference scheme finds larger values for the total number of social contacts  $k$  than previously reported [25] for the time period before NPIs were put in place. Superspreading events, which are not explicitly part of our model, can explain this discrepancy. A recent study which used mobility network data to show that the spread of the disease is mostly driven by infections at events, which connect different communities, for example in restaurants and religious establishments, further supports the importance of non-local contacts [28]. Moreover, empirical studies of the circumstances under which people got infected revealed that although 46 to 66 % of transmission is household-based (local contacts), non-local contacts between these cliques are essential to sustain the epidemic, even if only a low percentage of infections are caused directly by them [29]. A theoretical study that investigated the effect of different social network-based distancing strategies, and showed that the most effective social distancing strategy is to restrict contacts to a single clique (local contacts), and to eliminate any contacts between the cliques (non-local contacts) [30]. We inferred that lifting contact restrictions in Germany after June 6 moved the disease dynamics back into the exponential regime. However, the effective reproduction number remained close to one, likely due to a strong seasonal effect on the transmission probability. This seasonal effect likely ended in October leading to a second fast exponential growth of cases. The German government responded with new NPIs in November, which reduced the effective reproduction number to a value around one again corresponding to a linear regime. Our analysis shows that NPIs can reduce the effective reproduction number to one by eliminating predominantly non-local contacts. These are contacts outside of clustered cliques like households and work places in restaurants, bars, and clubs. However, eliminating the disease does most likely require to cut almost all contacts between different cliques, for example by working from home and not having direct contact with colleagues. In summary, government interventions should target non-local contacts in order to efficiently prevent disease spread.

## Acknowledgements

We thank Prof. Jan Hasenauer for valuable discussions and input about Bayesian parameter inference. We thank the Centre for Information Services and High Performance Computing at Technische Universität Dresden for providing high-performance computing infrastructure. Diana David-Rus thanks Prof. Manfred Wildner and the Department of Infectious Diseases Epidemiology Surveillance and Task Force at LGL-Bavaria for their support in ensuring the right infrastructure. **Funding:** S. S. is supported by the European Social Fund (ESF), co-financed by tax funds on the basis of the budget adopted by the members of the Saxon State Parliament. Y. S. is supported by the German Federal Ministry of Education and Research (FitMultiCell; grant number 031L0159A). H. H. is supported by the Volkswagen Foundation within the *Life?* program (grant number 96732).

**Author contributions:** Simon Syga: Conceptualization, Methodology, Software,

---

Formal analysis, Investigation, Data Curation, Writing - Original Draft, Visualization  
**Diana David-Rus:** Resources, Writing - Review & Editing **Yannik Schälte:**  
Software, Writing - Review & Editing **Michael Meyer-Hermann:** Writing - Review  
& Editing **Haralampos Hatzikirou:** Conceptualization, Methodology, Resources,  
Writing - Review & Editing **Andreas Deutsch:** Conceptualization, Methodology,  
Writing - Review & Editing, Supervision

**Competing interests:** The authors do not have competing interests.

**Data and materials availability:** All data is available in the manuscript or the  
supplementary materials. The simulation code is available as a Zenodo snapshot at  
<https://doi.org/10.5281/zenodo.4306105>.

## References

1. Matthias Buchholz an der Heiden and Osamah Hamouda. Schätzung der aktuellen Entwicklung der SARS-Cov-2-Epidemie in Deutschland - Nowcasting [Estimate of the current development of the SARS Cov-2 epidemic in Germany - Nowcasting]. *Epidemiol. Bull.*, 17(April):10–16, 2020.
2. Jonas Dehning, Johannes Zierenberg, F. Paul Spitzner, Michael Wibral, Joao Pinheiro Neto, Michael Wilczek, and Viola Priesemann. Inferring change points in the spread of COVID-19 reveals the effectiveness of interventions. *Science*, 369(6500):eabb9789, jul 2020.
3. Seth Flaxman, Swapnil Mishra, Axel Gandy, H Juliette T Unwin, Thomas A Mellan, Helen Coupland, Charles Whittaker, Harrison Zhu, Tresnia Berah, Jeffrey W Eaton, Mélodie Monod, Azra C Ghani, Christl A Donnelly, Steven Riley, Michaela A C Vollmer, Neil M Ferguson, Lucy C Okell, and Samir Bhatt. Estimating the effects of non-pharmaceutical interventions on COVID-19 in Europe. *Nature*, 584(7820):257–261, aug 2020.
4. W. O. Kermack and A. G. McKendrick. A contribution to the mathematical theory of epidemics. *Proc. R. Soc. London. Ser. A, Contain. Pap. a Math. Phys. Character*, 115(772):700–721, aug 1927.
5. Benjamin Ridenhour, Jessica M. Kowalik, and David K. Shay. Unraveling R 0 : Considerations for Public Health Applications. *Am. J. Public Health*, 104(2):e32–e41, feb 2014.
6. Neil M Ferguson, Daniel Laydon, Gemma Nedjati-Gilani, Natsuko Imai, Kylie Ainslie, Marc Baguelin, Sangeeta Bhatia, Adhiratha Boonyasiri, Zulma Cucunubá, Gina Cuomo-Dannenburg, Amy Dighe, Iaria Dorigatti, Han Fu, Katy Gaythorpe, Will Green, Arran Hamlet, Wes Hinsley, Lucy C Okell, Sabine Van Elsland, Hayley Thompson, Robert Verity, Erik Volz, Haowei Wang, Yuanrong Wang, Patrick GT Walker, Caroline Walters, Peter Winskill, Charles Whittaker, Christl A Donnelly, Steven Riley, and Azra C Ghani. Impact of non-pharmaceutical interventions (NPIs) to reduce COVID-19 mortality and healthcare demand. Technical report, Imperial College London, 2020.
7. Tom Britton, Frank Ball, and Pieter Trapman. A mathematical model reveals the influence of population heterogeneity on herd immunity to SARS-CoV-2. *Science*, 369(6505):846–849, aug 2020.
8. Stefan Thurner, Peter Klimek, and Rudolf Hanel. A network-based explanation of why most COVID-19 infection curves are linear. *Proc. Natl. Acad. Sci.*, 117(37):22684–22689, sep 2020.

- 
9. Duncan J Watts and Steven H Strogatz. Collective dynamics of ‘small-world’ networks. *Nature*, 393(6684):440–442, jun 1998.
  10. Albert-László Barabási and Eric Bonabeau. Scale-Free Networks. *Sci. Am.*, 288(5):60–69, may 2003.
  11. Matt J. Keeling, Leon Danon, Ashley P. Ford, Thomas House, Chris P. Jewell, Gareth O. Roberts, Joshua V. Ross, and Matthew C. Vernon. Networks and the epidemiology of infectious disease. *Interdiscip. Perspect. Infect. Dis.*, 2011, 2011.
  12. Romualdo Pastor-Satorras, Claudio Castellano, Piet Van Mieghem, and Alessandro Vespignani. Epidemic processes in complex networks. *Rev. Mod. Phys.*, 87(3):925–979, 2015.
  13. Christopher Wolfram. An Agent-Based Model of COVID-19. *Complex Syst.*, 29(1):87–105, apr 2020.
  14. Romualdo Pastor-Satorras and Alessandro Vespignani. Epidemic Spreading in Scale-Free Networks. *Phys. Rev. Lett.*, 86(14):3200–3203, apr 2001.
  15. Romualdo Pastor-Satorras and Alessandro Vespignani. Epidemic dynamics in finite size scale-free networks. *Phys. Rev. E - Stat. Physics, Plasmas, Fluids, Relat. Interdiscip. Top.*, 65(3):1–4, 2002.
  16. Y. Moreno, R. Pastor-Satorras, and A. Vespignani. Epidemic outbreaks in complex heterogeneous networks. *Eur. Phys. J. B*, 26(4):521–529, apr 2002.
  17. Michael Small and Chi K. Tse. Small world and scale free model of transmission of SARS. *Int. J. Bifurcat. Chaos*, 15(5):1745–1755, 2005.
  18. Natalia L. Komarova, Luis M. Schang, and Dominik Wodarz. Patterns of the COVID-19 pandemic spread around the world: exponential versus power laws. *J. R. Soc. Interface*, 17(170):20200518, sep 2020.
  19. Amanda Minter and Renata Retkute. Approximate Bayesian Computation for infectious disease modelling. *Epidemics*, 29(August):100368, dec 2019.
  20. Ensheng Dong, Hongru Du, and Lauren Gardner. An interactive web-based dashboard to track COVID-19 in real time. *Lancet Infect. Dis.*, 20(5):533–534, may 2020.
  21. Natalie Linton, Tetsuro Kobayashi, Yichi Yang, Katsuma Hayashi, Andrei Akhmetzhanov, Sung-mok Jung, Baoyin Yuan, Ryo Kinoshita, and Hiroshi Nishiura. Incubation Period and Other Epidemiological Characteristics of 2019 Novel Coronavirus Infections with Right Truncation: A Statistical Analysis of Publicly Available Case Data. *J. Clin. Med.*, 9(2):538, feb 2020.
  22. Google. Germany, March 29, 2020 Mobility changes. Technical report, Google, 2020.
  23. Qin-Long Jing, Ming-Jin Liu, Zhou-Bin Zhang, Li-Qun Fang, Jun Yuan, An-Ran Zhang, Natalie E. Dean, Lei Luo, Meng-Meng Ma, Ira Longini, Eben Kenah, Ying Lu, Yu Ma, Neda Jalali, Zhi-Cong Yang, and Yang Yang. Household secondary attack rate of COVID-19 and associated determinants in Guangzhou, China: a retrospective cohort study. *Lancet Infect. Dis.*, 20(10):1141–1150, oct 2020.

- 
24. Hendrik Streeck, Bianca Schulte, Beate Kuemmerer, Enrico Richter, Tobias Hoeller, Christine Fuhrmann, Eva Bartok, Ramona Dolscheid, Moritz Berger, Lukas Wessendorf, Monika Eschbach-Bludau, Angelika Kellings, Astrid Schwaiger, Martin Coenen, Per Hoffmann, Markus Noethen, Anna-Maria Eis-Huebinger, Martin Exner, Ricarda Schmithausen, Matthias Schmid, and Gunther Hartmann. Infection fatality rate of SARS-CoV-2 infection in a German community with a super-spreading event. *Nat. Commun.*, pages 1–12, 2020.
  25. Joël Mossong, Niel Hens, Mark Jit, Philippe Beutels, Kari Auranen, Rafael Mikolajczyk, Marco Massari, Stefania Salmaso, Gianpaolo Scalia Tomba, Jacco Wallinga, Janneke Heijne, Malgorzata Sadkowska-Todys, Magdalena Rosinska, and W. John Edmunds. Social Contacts and Mixing Patterns Relevant to the Spread of Infectious Diseases. *PLoS Med.*, 5(3):e74, mar 2008.
  26. Dirk Brockmann and Dirk Helbing. The Hidden Geometry of Complex, Network-Driven Contagion Phenomena. *Science*, 342(6164):1337–1342, dec 2013.
  27. R. A. Fisher. The wave of advance of advantageous genes. *Ann. Eugen.*, 7(4):355–369, jun 1937.
  28. Serina Chang, Emma Pierson, Pang Wei Koh, Jaline Gerardin, Beth Redbird, David Grusky, and Jure Leskovec. Mobility network models of COVID-19 explain inequities and inform reopening. *Nature*, nov 2020.
  29. Elizabeth C Lee, Nikolas I Wada, M Kate Grabowski, Emily S Gurley, and Justin Lessler. The engines of SARS-CoV-2 spread. *Science*, 370(6515):406–407, oct 2020.
  30. Per Block, Marion Hoffman, Isabel J. Raabe, Jennifer Beam Dowd, Charles Rahal, Ridhi Kashyap, and Melinda C. Mills. Social network-based distancing strategies to flatten the COVID-19 curve in a post-lockdown world. *Nat. Hum. Behav.*, 4(6):588–596, jun 2020.
  31. Emmanuel Klinger, Dennis Rickert, and Jan Hasenauer. pyABC: distributed, likelihood-free inference. *Bioinformatics*, 34(20):3591–3593, oct 2018.
  32. Nick Jagiella, Dennis Rickert, Fabian J. Theis, and Jan Hasenauer. Parallelization and high-performance computing enables automated statistical inference of multi-scale models. *Cell Systems*, 4(2):194 – 206.e9, 2017.

## Supporting Information

### Model definition

We study an agent-based, discrete-time SEIR-like model on the classical Watts-Strogatz small world network, representing agents as network nodes. The network is constructed by, first, connecting every node with its  $k$  nearest neighbors in a ring-like topology, and, second, rewiring every link to a random node with probability  $p$ . A sketch of the network can be found in Fig. S1. Every node  $i$  has a discrete state  $s_i \in \mathcal{S} = \{S, E, I, R\}$ , corresponding to susceptible ( $S$ ), exposed ( $E$ ), infectious ( $I$ ), and removed ( $R$ ) states.

Disease progression is dictated by  $\Gamma$ -distributed waiting times inferred from COVID-19 disease characteristics, as these have been found to describe the disease best [21]. During every discrete time step  $t$ , where the length of the time step

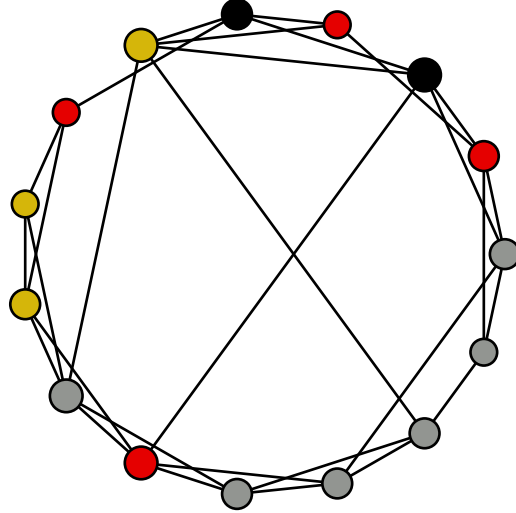


**Figure S1. Watts-Strogatz small world network.** Agents are placed in a ring-like topology and linked to their  $k$  nearest neighbors. Next, every link is rewired randomly with a small probability  $p$ . Every agent has one of four states: susceptible (gray), exposed (gold), infectious (red) or removed (black). The size of network nodes corresponds to the node degree.

corresponds to 1 day, each susceptible agent can become exposed with probability  $p_I$  to every infectious agent they are connected to,

$$P(s_i(t+1) = E | s_i(t) = S) = 1 - (1 - p_I)^{I_i}, \quad (3)$$

where  $I_i$  is the number of infectious agents node  $i$  is connected to. Upon infection, we change the agent's state to exposed, and assign a waiting time  $\tau_E \sim \Gamma(k_E, \theta_E)$  which we draw from a  $\Gamma$ -distribution with shape  $k_E$  and scale  $\theta_E$ . During every time step, waiting times are reduced by 1,  $\tau_E(t+1) = \tau_E(t) - 1$  if  $\tau_E(t) > 0$ . Else, the disease progresses,  $s_i(t+1) = I$ , and a new waiting time is assigned from another  $\Gamma$ -distribution  $\tau_I \sim \Gamma(k_I, \theta_I)$ , with shape  $k_I$  and scale  $\theta_I$ . Finally, when  $\tau_I \leq 0$ , the node is removed,  $s_i(t+1) = R$ . A sketch for the SEIR dynamics can be found in Fig. S2. We calculate the shape and scale of the  $\Gamma$ -distributions from the reported mean time and variance in the respective states according to

$$k_{E,I} = \frac{\langle \tau_{E,I} \rangle^2}{\langle \Delta \tau_{E,I}^2 \rangle}, \quad (4)$$

$$\theta_{E,I} = \frac{\langle \Delta \tau_{E,I}^2 \rangle}{\langle \tau_{E,I} \rangle}. \quad (5)$$

Note that we did not infer these parameters with our Bayesian parameter inference framework.

In our model we do not account for an inflow of infectious people by travel; we instead account for the initial surge of infections by placing randomly  $n_E(0)$  exposed and  $n_I(0)$  infectious agents in the population.

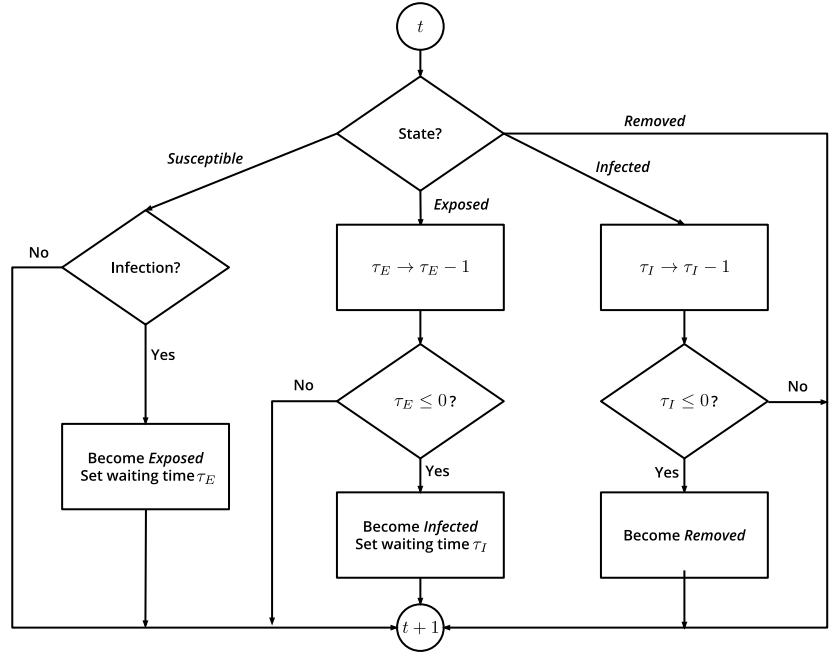


**Figure S2. Dynamics in the agent-based SEIR model.** Susceptible agents can become exposed, if they are linked to infectious agents (see text). Exposed agents become infectious after the waiting time  $\tau_E$ , and infectious agents are removed after  $\tau_I$ . All nodes are updated simultaneously at every time step  $t$ .

## Bayesian parameter inference

### General approach

We apply approximate Bayesian computation with a sequential Monte-Carlo scheme (ABC-SMC) to infer the set of parameters  $\Theta = \{p_I, p, k, n_E(0), n_I(0)\}$  of our agent-based model. We always keep the total number of agents fixed at  $n = 3 \cdot 10^5$ . To this end, we employ the Python package pyABC [31]. In short, the algorithm employs sequential importance sampling over generations  $T = 1, \dots, n_T$ . In generation  $T$ , the algorithm draws sets of parameters  $\theta_i$  from a given proposal distribution and consequently simulates data  $C^{(i)}$  from the model, until  $n_{\text{ABC}}$  instances were accepted based on the comparison to observed data via a distance function  $D(C^{(i)}, C_{\text{obs}})$  and acceptance threshold  $\epsilon_T$ ,  $D(C^{(i)}, C_{\text{obs}}) \leq \epsilon_T$ . As distance function, we choose the absolute difference between new cases in the model instance  $C^{(i)}(t)$  and the respective reports for Germany  $C_{\text{obs}}(t)$ ,

$$D(C^{(i)}, C_{\text{obs}}) := \sum_t \left| C^{(i)}(t) - C_{\text{obs}}(t) \right|. \quad (6)$$

New cases in the model are given by the daily new infections

$$C^{(i)}(t) = n_I^{(i)}(t) - n_I^{(i)}(t-1) + n_R^{(i)}(t) - n_R^{(i)}(t-1). \quad (7)$$

They are compared to the seven-day rolling average of new case reports in Germany  $C_{\text{obs}}(t)$  provided by John Hopkins University [20] to account for the weekly fluctuation in reporting. Acceptance of model instances depends on the acceptance threshold  $\epsilon_T$  of generation  $T$ , which we choose as the median of the distances of the accepted distances of the previous generation

$$\epsilon_{T+1} = \text{median} \left( \left\{ D(C^{(i)}, C_{\text{obs}}) < \epsilon_T \right\} \right). \quad (8)$$

When  $n_{ABC}$  model instances have been accepted, the algorithm constructs new proposal distributions from the accepted instances to allow high acceptance rates while decreasing the threshold [32]. In particular, for the continuous variables it employs a multivariate normal distribution with adaptive covariance matrix based on the sample covariance matrix, whose scale parameter is determined by a grid search with 5-fold cross validation and refitting on the whole data set. We compute the discrete numbers of initially exposed and infectious people  $n_E(0), n_I(0)$  by rounding the continuous output of the multivariate normal distribution. We can do this without a large error as these parameters vary smoothly over a large range. For the parameter  $k$  we employ an adaptive, discrete transition that assigns probabilities to all possible parameter values directly from the frequency of the respective value in the population of accepted particles with additional random jumps (with probability 0.3) to ensure absolute continuity of the prior..

The process is repeated until the acceptance threshold is sufficiently low; we especially ensured that the threshold is considerably lower than the difference between the reported cases and the seven-day rolling average of cases.

### February 26 - March 15

The early phase of the epidemic is characterized by a low number of cumulative infections. We can therefore directly use the absolute numbers of new infections as input for our agent-based model, as we are always far away from the epidemic threshold. We choose broad, uniform priors for all the parameters that can be found in table S1. Note that the probability for random connections varies on several orders of magnitude  $p \in [10^{-6}, 10^0]$  and we therefore infer this parameter on a logarithmic scale. We use  $n_{ABC} = 100$  and obtain an effective sample size of  $n_{\text{eff}} \approx 46$ .

**Table S1.** Priors of model parameters for the time period February 26 to March 15.

Parameter	Variable	Prior distribution
Infection probability	$p_I$	Uniform(0.01,0.07)
Probability of random links	$\log_{10} p$	Uniform(0,-6)
Number of links	$k/2$	DiscreteUniform(1,16)
Initially exposed	$n_E(0)$	Uniform(0,47)
Initially infectious	$n_I(0)$	Uniform(0,160)

### March 16 - June 6

In the time period from March 16 to June 6 Germany recorded 177652 cases in total. This means that it becomes computationally unfeasible to replicate the population directly in our model without noticing a strong effect of the removed (immune) agents. Therefore, we scale down the total number of infections to our system size and compare the relative number of cases per 300,000 people instead. Assuming our hypothesis that the NPIs lead to a strongly clustered transmission network holds, we expect a large number of unconnected communities in Germany in that time period, which we represent as distinct model instances. We use  $n_{ABC} = 200$  and obtain an effective sample size of  $n_{\text{eff}} \approx 105$ .

### June 7 - September 15

To infer the parameters of the system during this time period we first sample parameters from the posterior distribution which we obtained for the previous time period, and let the system evolve for 81 days (corresponding to the time period from

**Table S2.** Priors of model parameters for the time period March 16 to June 6.

Parameter	Variable	Prior distribution
Infection probability	$p_I$	<code>Uniform(0.01,0.03)</code>
Probability of random links	$\log_{10} p$	<code>Uniform(0,-6)</code>
Number of links	$k/2$	<code>DiscreteUniform(1,11)</code>
Initially exposed	$n_E(0)$	<code>Uniform(3,57)</code>
Initially infectious	$n_I(0)$	<code>Uniform(38,414)</code>

March 16 to June 6). Next, we change the infection probability  $p_I$  and assign a new transmission network based on a new set of parameters  $p, k$ . For these parameters, we choose the same prior distributions as for the previous time period, see Table S3. We use  $n_{ABC} = 200$  and obtain an effective sample size of  $n_{\text{eff}} \approx 164$ .

**Table S3.** Priors of model parameters for the time period June 7 to September 15.

Parameter	Variable	Prior distribution
Infection probability	$p_I$	<code>Uniform(0.01,0.03)</code>
Probability of random links	$\log_{10} p$	<code>Uniform(0,-6)</code>
Number of links	$k/2$	<code>DiscreteUniform(1,11)</code>

## Parameter scan

To investigate the disease dynamics in the small-world network, we perform a parameter scan. We vary the network parameters  $p, k$  while keeping the rest of the parameters fixed at  $n = 10^5, p_I = 0.02, n_E(0) = 0, n_I(0) = 10$ . Our choice for  $p_I$  during the parameter scan is motivated by reports of the COVID-19 individual-level secondary attack rate (SAR) in the household of 17 % [23]. Inverting eq. 3 we obtain

$$p_I = 1 - \sqrt[3]{1 - SAR} \approx 0.02. \quad (9)$$

We vary the number of contacts from  $k = 2, 4, \dots, 24$  and sample the probability for random contacts in eleven equally-spaced steps on the log scale from  $\log_{10} p = -5, \dots, 0$ . As initial condition, 10 random agents are set to the infectious state and the system is simulated until there are no more exposed and infectious agents. We repeat this process five times per parameter combination  $(p, k)$ . As output we determine the peak of simultaneously infectious people

$$n_{\text{peak}}(p, k) := \max_t n_I(t, p, k), \quad (10)$$

and the cumulative infection curves

$$N(t, p, k) = n_I(t, p, k) + n_R(t, p, k). \quad (11)$$

In the highly clustered regime  $p = 10^{-5}$  we calculate the linear growth rate from the cumulative infections as

$$c(k) := \left\langle \frac{N(t_{\text{max}}, k) - N(t_{\text{min}}, k)}{t_{\text{max}} - t_{\text{min}}} \right\rangle, \quad (12)$$

where we neglect the initial exponential growth by skipping  $t_{\text{min}} = \langle \tau_I \rangle = 10$  time steps.

## Mathematical analysis

### Epidemic threshold

We can calculate an upper bound for the number of contacts  $k_c$  by demanding  $R_0 = 1$ , i. e. a single infectious person in a network of susceptible people will effect on average one other person. Using eq. 3 we can calculate the expected number of infections as

$$R_0 = 1 = k_c [1 - (1 - p_I)^{\tau_I}] \iff k_c = \frac{1}{1 - (1 - p_I)^{\tau_I}}. \quad (13)$$

For  $p_I = 0.02$  and  $\langle \tau_I \rangle \approx 10$  we obtain  $k_c \approx 5.5$ .

### Derivation of differential-equation approximation

In order to predict the linear growth of infections in the highly clustered small-world network, we consider a simplified variant of our original model, where we neglect the exposed state and assume that the progression times are distributed exponentially. Then we describe the state of an agent  $j$  in our model by a set of three Boolean stochastic variables  $s_j(t), i_j(t), r_j(t) = 0, 1$ , where  $s_j + i_j + r_j = 1$  and  $s_j = 1$  indicates that the agent is susceptible,  $i_j = 1$  means he is infectious and if  $r_j = 1$  he is removed. We represent the event "agent  $j$  becomes infectious at time  $t$ " by the Boolean stochastic variable  $\alpha_j(t)$  with

$$P(\alpha_j(t) = 1) = 1 - (1 - p_I)^{I_j(t)}, \quad (14)$$

where  $I_j(t) := \sum_{m \in \mathcal{N}_j} i_m(t)$  is the number of infectious agents in the neighborhood  $\mathcal{N}_j$  of agent  $j$ . Similarly, the event "agent  $j$  is removed at time  $t$ " is given by the stochastic variable  $\beta_j(t)$  with

$$P(\beta_j(t) = 1) = p_R = 1/\tau_I. \quad (15)$$

During one time step the state of all agents changes as

$$s_j(t+1) = s_j(t) - \alpha_j(t)s_j(t), \quad (16)$$

$$i_j(t+1) = i_j(t) + \alpha_j(t)s_j(t) - \beta_j(t)i_j(t), \quad (17)$$

$$r_j(t+1) = r_j(t) + \beta_j(t)i_j(t). \quad (18)$$

We want to calculate the expected value of the state variable under a mean-field approximation, i. e. we replace the expected value of a function  $f(X)$  of any random variable  $X$  by the function evaluated at the expected value of the random variable,  $\langle f(X) \rangle \approx f(\langle X \rangle)$ . In particular, this also means that we neglect any correlations between the state variables of neighboring nodes. We denote the expected values of the state variables as  $\sigma_j(t) := \langle s_j(t) \rangle$ ,  $\iota_j(t) := \langle i_j(t) \rangle$ ,  $\rho_j := \langle r_j(t) \rangle$ . For the expected number of infectious neighbors we obtain

$$\langle I_j(t) \rangle = (1 - p) \sum_{m=-k/2}^{k/2} \iota_m(t) + \frac{kp}{N-1} \sum_{m \neq j} \iota_m(t), \quad (19)$$

where  $N$  is the total number of nodes in the network and  $p$  is the probability of a random link (see Model definition). We also introduce a small time step length  $\tau > 0$  and the continuous time  $\hat{t} = \tau t$  along with the transition rates  $\kappa_I := p_I/\tau$ ,  $\kappa_R := p_R/\tau$ . In the following we only consider the continuous time and drop the hat for better readability. For  $\tau \rightarrow 0$  we can then approximate the expected value of  $\alpha_j(t)$  by a Taylor approximation around  $p_I = 0$  as

$$P(\alpha_j(t) = 1) = 1 - (1 - \kappa_I \tau)^{I_j(t)} \approx \kappa_I \tau I_j(t). \quad (20)$$

Approximating all time-dependent functions by their Taylor approximation up to first order  $f(t + \tau) \approx f(t) + \tau f'(t)$  and rearranging terms we obtain the following set of non-linear ODEs for the expected value of the agents' states

$$\sigma'_j(t) = -\kappa_I \sigma_j(t) \langle I_j(t) \rangle, \quad (21)$$

$$\iota'_j(t) = \kappa_I \sigma_j(t) \langle I_j(t) \rangle - \kappa_R \iota_j(t), \quad (22)$$

$$\rho'_j(t) = \kappa_R \iota_j(t). \quad (23)$$

Note that this set of ODEs does not depend on the time step length any more and that the equations are linked by the expected number of infected in every node's neighborhood given by eq. 19. We can further simplify our system by considering the regime  $N \rightarrow \infty$ , and introducing the spatial step length  $\Delta x > 0$  so that  $N\Delta x = L = \text{const}$ . We can then replace the state probabilities  $\sigma_j(t), \iota_j(t), \rho_j(t)$  by the probability densities  $\sigma(x + j\Delta x, t), \iota(x + j\Delta x, t), \rho(x + j\Delta x, t)$ . This allows us to approximate the expected number of infectious agents in the neighborhood by expanding the terms  $\iota(x + m\Delta x, t) \approx \iota(x, t) + m\Delta x \partial_x \iota(x, t) + m\Delta x/2 \partial_{xx} \iota(x, t)$  to obtain

$$\begin{aligned} \langle I_j(t) \rangle &= (1-p) \sum_{m=-k/2}^{k/2} \iota_m(t) + \frac{kp}{N-1} \sum_{m \neq j} \iota_m(t) \approx \\ &\approx (1-p)k \left( \iota(x, t) + \tilde{k} \partial_{xx} \iota(x, t) \right) + \frac{kp}{L} \int_0^L \iota(x, t) dx, \end{aligned} \quad (24)$$

where  $\tilde{k} := \Delta x k(k+1)(2k+1)/12$ . Finally, with  $I(t) := 1/L \int_0^L \iota(x, t) dx$  as the total number of infectious people, we obtain the following set of PDEs

$$\partial_t \sigma(x, t) = -\kappa_I k \sigma_j(x, t) \left[ (1-p) \left( \iota(x, t) + \tilde{k} \partial_{xx} \iota(x, t) \right) + pI(t) \right], \quad (25)$$

$$\partial_t \iota(x, t) = \kappa_I k \sigma_j(x, t) \left[ (1-p) \left( \iota(x, t) + \tilde{k} \partial_{xx} \iota(x, t) \right) + pI(t) \right] - \kappa_R \iota(x, t), \quad (26)$$

$$\partial_t \rho(x, t) = \kappa_R \iota(x, t). \quad (27)$$

### Calculation of the infection wave speed in the small-world network

To calculate the wave speed of infections we consider the regime  $p = 0$ , so that we can neglect the non-local coupling by  $I(t)$  in eq. 25. We also notice that there are two steady states  $\sigma = 1$  and  $\rho = 1$ , and we suspect that they are connected by a travelling wave, as the first steady state is unstable while the second one is stable if  $k\kappa_I > \kappa_R$ . Next we make the wave ansatz  $\iota(x, t) = \iota(z = x - ct)$  with the wave speed  $c$ . For  $z \rightarrow \infty$  (far from the wave front) we expect  $\rho \rightarrow 0, \sigma \rightarrow 1$  and we can therefore write eq. 26 as

$$-c\iota' = \kappa_I k \left( \iota + \tilde{k} \iota'' \right) - \kappa_R \iota. \quad (28)$$

This linear, homogeneous ODE with constant coefficients has the characteristic polynomial

$$\kappa_I k \tilde{k} \gamma^2 + c\gamma + (k\kappa_I - \kappa_R) = 0, \quad (29)$$

with the solutions

$$\gamma_{1/2} = \frac{-c \pm \sqrt{c^2 - 4\kappa_I k \tilde{k} (k\kappa_I - \kappa_R)}}{2\kappa_I k \tilde{k}}. \quad (30)$$

We only find non-oscillatory solutions for wave speeds

$$c \geq \sqrt{4\kappa_I k \tilde{k} (k\kappa_I - \kappa_R)} =: c_{\min} \propto k^2 \sqrt{\tilde{k}}. \quad (31)$$